Nano-viscosity of supercooled liquid measured by fluorescence correlation spectroscopy: pressure and temperature dependence and the density scaling

G. Meier[1], J. Gapinski[2,3], M. Ratajczyk[2], M. P. Lettinga[1], K. Hirtz[4], E. Banachowicz[2], and A. Patkowski[2,3]

[1]*ICS3, Weiche Materie, FZ-Jülich, Postfach 1913, 52428 Jülich, Germany*

[2] *Faculty of Physics, A. Mickiewicz University, Umultowska 85, 61-614 Poznan, Poland*

[3]*NanoBioMedical Centre A. Mickiewicz University, Umultowska 85, 61-614 Poznan, Poland*

[4]*PGI-JCNS, FZ-Jülich, Postfach 1913, 52428 Jülich, Germany*

Abstract

Single particle experiments: fluorescence correlation spectroscopy (FCS) and particle tracking (PT) allow to obtain the nano-viscosity of the system from the measured self/tracer translational diffusion coefficients, using the Stokes-Einstein (SE) relation. In order to perform such measurements as function of pressure and temperature a new sample cell was designed and is described in this work. We show that this cell in combination with a long working distance objective of the confocal microscope can be used for successful FCS, PT and confocal imaging experiments in broad pressure (0.1-100 MPa) and temperature ranges. The temperature and pressure dependent nano-viscosity of a van der Waals liquid obtained from the translational diffusion coefficient measured in this cell by means of FCS obeys the same scaling as the rotational relaxation and macro-viscosity of the system.

Keywords: Confocal Microscopy, High Pressure, Self-Diffusion, Tracer-Diffusion, Particle Tracking, Fluorescence Correlation Spectroscopy (FCS), Density Scaling

1. Introduction

Glass is a material commonly occurring in nature, technology and everyday life. It can be obtained from a supercooled liquid by decreasing temperature T or increasing pressure P. The liquid-glass transition is not a typical thermodynamic 1-st or 2-nd order transition and is usually defined by conditions at which the structural relaxation times of the liquid (are frozen) exceed the time of the experiment. For convenience, in the case of molecular glass forming liquids, it is defined by the P and T values at which the structural relaxation times become larger than 100 s. Despite extensive theoretical and experimental studies over many years the dynamics of supercooled liquids, with relaxation times increasing by more than 13 orders of magnitude in a narrow T-range (or P-range) between the melting and glass transition temperatures, and the glass transition are not fully understood. They remain one of the main challenges of the condensed matter physics. One of the important and unusual features of the dynamics of supercooled liquids is its heterogeneity. In recent years it has been studied theoretically [1] but the experimental evidence remains very scarce [2, 3]. It mainly comes from the studies on a single molecule level [3, 4] which are possible by means of fluorescence techniques like Fluorescence Correlation Spectroscopy (FCS) and Particle Tracking (PT) in which fluorescence microscopes are used in confocal (FCS) or epi (PT) geometries.

The combination of microscopy and high pressure is challenging and technically difficult since the main requirements for high resolution microscopy and for applying high pressure are in conflict. High mechanical resistance needed for high pressure automatically leads to an extended size of the sample environment (cell window), while the working distance for the microscope objective needs to be minimal to assure maximum resolution and efficiency.

High pressure FCS experiments offer very attractive possibilities to study pressure dependence of the dynamics of glass forming liquids and interactions in living cells. From the self/tracer diffusion coefficient of the fluorescent probe measured by means of FCS, the

viscosity of the system can be determined using the Stokes-Einstein (SE) relation. It is usually very difficult to measure the viscosity of a supercooled liquid in broad temperature and pressure (T, P) ranges. In our previous publication [5] we demonstrated the feasibility of the measurements of the viscosity of such liquids by means of FCS in a broad T-range. In this work we extend the field of applicability of FCS to pressure dependent studies and discuss the T and P dependent dynamic data.

Although dynamic properties and transport coefficients of glass forming liquids depend equally on temperature T and pressure P, traditionally the experiments are performed under the isobaric (P = const, T-variable) conditions and much less frequently when both T and P are changed. The experimental data is usually presented in the isobaric or isothermal (T = const, P-variable) representations. In order to simultaneously consider the dependence on both T and P, a scaling function $f(T\rho^{-\gamma})$ depending only on the scaling parameter $T\rho^{-\gamma}$ is used, where ρ is the density and γ is a material constant. Thus, we use the scaling relation which projects the data obtained in the whole studied (P, T) space onto a single line described by the scaling function $f(T\rho^{-\gamma})$ with an obvious prerequisite that the $\rho(P,T)$ data are available for the studied substance.

It was demonstrated that for ortho-terphenyl (OTP) the density scaling works, i.e. the reduced reorientational relaxation time and viscosity can be scaled to a single curve when plotted versus $T\rho^{-5.35}$ when the correct equation of state (EoS) is used to calculate the T and P dependence of the density [6]. In the previous studies on OTP [7] when another equation of state was used a successful scaling of the same data was achieved with the exponent γ equal to about 4.

In this work we show that for OTP and OTP/BMPC mixture (BMPC - 1,1'-di(p-methoxyphenyl)cyclohexane) also the translational motion measured at different T and P conditions can be scaled with the same scaling function and exponent γ as for viscosity and

rotational dynamics in the temperature range $T > 1.2\,T_g$, where in this case T_g must be considered as a pressure dependent quantity.

The first working high pressure microscopy cells were developed by Hartmann *et al.* [8] and Müller and Gratton [9]. The first cell worked fine up to 300 MPa producing correct microscopic pictures but no FCS experiments were performed. Moreover, the sample loading and environment change procedures seemed to be complicated. Since sapphire was used as optical window, the birefringence effects were unavoidable. Substantial thickness of the window that could withstand 300 MPa pressure resulted in a poor quality of microscopic images [10] despite the use of long working distance objectives with correction collars. The second cell [9] was a capillary high pressure cell with the pressure range of 0-300 MPa . This cell was dedicated only to FCS.

Two other high pressure cells for imaging using high resolution microscopy were developed by Vass *et al.* [11, 12]. The first one [11] could cover the pressure range up to 700 MPa. The pressure cell window was made of a 0.5 mm thick diamond or 0.45 mm thick quartz plate. With a long working distance (LWD) objective this pressure cell was used for high resolution imaging. In the second cell [12] a 0.2 mm thick quartz window was fixed by a layer of adhesive to the outside of the cell. Imaging of single fluorescence molecules at the inner surface of the window was performed by means of total internal reflection fluorescence (TIRF) under high pressures. In both cases no FCS experiment were performed with those cells.

Our experience in designing high pressure cells for optical experiments resulted in constructing three cells, each of them dedicated to a different kind of experiment: birefringence [13], simultaneous neutron and light scattering [14] and dynamic/Brillouin light scattering [15]. Due to thick windows none of them allowed for using high quality objectives and hence could not be used for FCS or PT experiments.

In this paper we report on a new design of a high pressure cell dedicated to FCS and high resolution microscopy measurements. A very simple O-ring construction is capable of containing the sample and separating it from the pressurizing medium. A 1 mm thick diamond window gives optical access to the sample and maintaines the mechanical resistance of the cell up to 100 MPa. The thickness of the metal part of the cell excludes the use of immersion objectives, however with the use of advanced long working distance objectives with a large correction range for cover glass thickness, an FCS experiment was possible and microscopic images of high quality could be obtained. As almost entire cell mass is the steel body, it was also relatively easy to include effective electrical heating which extended the temperature range from ambient to ~100°C. Our construction was meant as a 'working prototype' or a 'prove of concept' to determine the direction in which the development should be made, as a lot of compromises had to be made in the design. Despite that, the cell turned out to be a successful construction.

A more advanced model of our cell could be used for investigation of living cells behavior at high pressure conditions. For example, *in situ* observations of microbial inactivation by high pressure application were demonstrated by Frey *et al.* [10], together with a complete overview of what is known in the field.

At the end of Introduction let us make a short digression concerning the term 'nano-viscosity'. In this manuscript the term "nano-viscosity" is used to indicate that this viscosity is calculated from the diffusion coefficient of a colloidal particle (a probe) using the SE relation under the assumption that the hydrodynamic radius remains practically constant upon T and P changes. As we have shown in our earlier publications [16, 17], in complex systems the nano-viscosity, for small probe sizes, is much smaller than the macro-viscosity (measured by means of rheological methods) and, eventually, they became equal when the probe size reaches a certain value. As in most cases this characteristic size remains in the nanometer

range, ‘nano-viscosity’ seems to be a proper term for such calculated property. However, it is not the absolute probe size that defines the transition from ‘nano-‘ to ‘macro-‘ viscosity but the ratio of the probe size to the characteristic size of the micro-structure of the complex medium. In principle, even a sub-micron size probe can ‘feel’ the nano-viscosity, much smaller than the rheological one, if only the internal structure of the medium is properly designed. Perhaps the term ‘Stokes-Einstein viscosity’ could also be used to describe our results, however we think that the word ‘nano’ better reflects the fact that in most cases only for nanometer size probes any deviation of such calculated viscosity from the rheological one can be found.

The paper is organized as follows: In the Materials and Methods section the construction/design of a new high pressure cell for confocal imaging and FCS is described. We also show that a successful FCS experiment can be performed using our new setup consisting of a high pressure cell with a 1 mm thick diamond window and a LWD objective equipped with the correction collar. Then the basic concepts of particle tracking (PT) and fluorescence correlation spectroscopy (FCS) are briefly summarized. In the Results and discussion section we present first the results of the confocal imaging using the new setup. Then the pressure and temperature dependent studies of translational diffusion of silica nanoparticles in ethanol and ethanol/water mixture using the new setup and particle tracking are presented. Next the results of the T and P dependent FCS measurements of the translational tracer diffusion coefficient D^T of a dye in OTP/BMPC mixture are shown. These D^T data for the mixture and our previously published data for OTP [5] are compared to the literature data on macroscopic viscosity and rotational diffusion using the concept of density scaling.

2. Materials and methods

2.1. Materials

PS-FluoGreen particles of 0.606 μm diameter were purchased from Micro Particles GmbH (Berlin, Germany), Lot PS-FluoGreen-Fi131.

Ortho-terphenyl (OTP) from Aldrich was distilled under vacuum. Its hydrodynamic radius amounts to 0.41 nm.

BMPC (1,1'-di(p-methoxyphenyl)cyclohexane) was synthesized according to procedure described in [18]. Its hydrodynamic radius 0.47 nm. The hydrodynamic radii for OTP and BMPC were calculated on the basis of their chemical structure and are given only for comparison with the corresponding values of the fluorescent probes.

Alexa488 was obtained from Alexa Fluor® 488 NHS ester, hydrodynamic radius 0.59 nm [19]. Alexa488 solution in toluene was prepared by diluting 1 mM Alexa488 water solution 1000× with methanol and then diluting the resultant solution 100× with toluene.

The 70/30 (by weight) OTP/BMPC mixture containing about 1 nM of Alexa488 was prepared by dissolving proper amounts of the components in toluene and then removing toluene by evaporation in a vacuum oven for several days.

The synthesis of octadecyl grafted silica spheres was done in two steps: first the cores were prepared according to Strober *et al.* [20] and then grafted with stearyl alcohol as first done by van Helden [21]. The radius determined by DLS [22] was 394 nm. In the experiments samples in ethanol and 50/50 (v/v) ethanol/water mixture were examined. The concentration of spheres amounted to 0.0025% v/v (stock solution diluted 2000 times).

2.2. The high pressure cell

The cell body is manufactured from Nimonic 90 alloy. The mechanical stability of the cell body is calculated to resist about 150 MPa. The weak point of every optical cell is the resistance of the window construction. For the diamond window opening in our geometry the

following relation was used to calculate the maximum pressure P_{max} that the window can withstand [23]:

$$P_{\max} = 3.6\frac{d^2 M_r}{f^2 s} \quad (1)$$

where d is the window thickness, f is the free opening diameter, M_r is a material constant (10 GPa for diamond) and s is the safety value. Using a safety value $s = 4$, $d = 1$ mm and $f = 3$ mm a maximum working pressure of P_{max} of 100 MPa was obtained for our set-up. The real maximum working pressure P_{max} is in fact higher since we use an extremely high value for s and our non-supported opening is smaller than 3 mm in diameter. A working pressure of about 100 MPa seems to be rather realistic and sufficient for most applications.

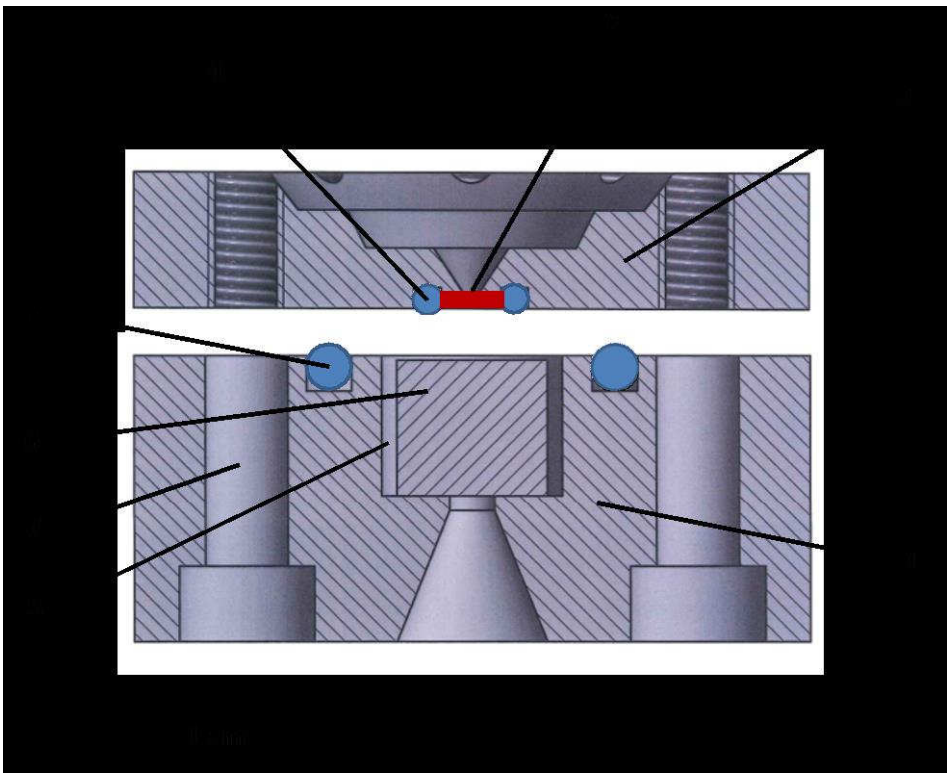

Figure 1. Schematic sketch of the cell. 1: cell body, 2: cover plate, 3: diamond window, 4: O-ring to embed the sample, 5: groove for the large O-ring, 6: sapphire/glass window, 7: holes for screws, 8: gap for pressurizing medium.

In Fig. 1 the schematic sketch of our cell is shown. The cell body and cover are held together by 8 screws M5, which press a Viton O-ring. The diameter of the cell is 45 mm. The top

cover bearing the diamond window leaves an opening for the microscope objective to come as close as possible to the sample. The thickness of the cover plate at that position is 4 mm.

What is not shown in Fig.1 is the inlet for the pressurizing medium (hydraulic oil or nitrogen), which is visualized in Fig. 2. The windows are glued to the supporting steel planes by superglue Loctite 408. Care has to be taken that the amount of glue used is so little that no glue will contaminate the optical surfaces. The gluing has two purposes: it seals the cell and helps to smooth the steel surfaces (surface roughness of about 5 μm). The sapphire window is somewhat less in height than the depth of the steel opening into which it is glued. That is why a very tiny O-ring (Viton 3×1) can be used just between the sapphire and the diamond. Assembling the cell with the sample is performed by: first, placing the small O-ring wetted with sample, to keep the O-ring in place only through adhesion, on the diamond, and second putting a relatively large drop of sample on the sapphire. Pressing now the two parts together provides a bubble free assembly, where the small O-ring contains the sample and is located centrally, such that the light path is not blocked. Through the gap next to the thick window (Fig. 1, element 8) hydraulic oil or nitrogen can access the small O-ring which transmits the pressure on to the sample, see Figs. 2a,b.

The cell is mounted on a microscope via a home-built *xy* stage. Connection to a hand driven piston type oil pressure generator (Nova-Swiss) is made via flexible high pressure tubing. The cell volume under pressure is of the order of 0.01 cm^3. It assures a rather steep increase of the pressure of the order of 20 MPa/s and can thus be used to perform pressure jump experiments. The cell and its mounting in the stage suitable for the microscope are shown in Fig. 2c. The sample can be also pressurized by nitrogen. In this case a compressor (NovaSwiss, Switzerland) is used instead of a piston pump.

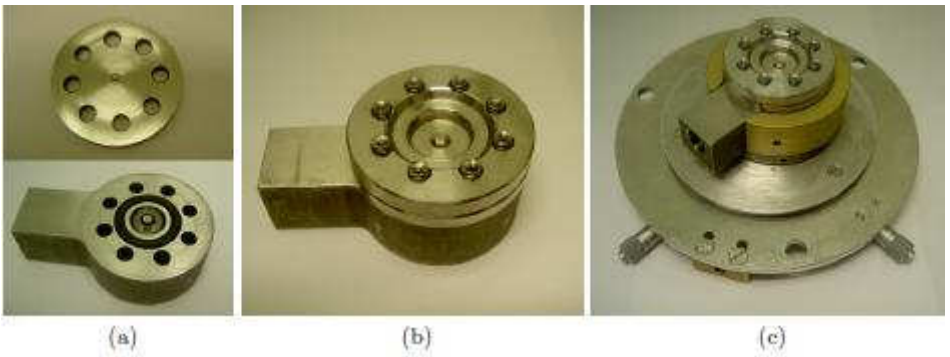

Figure 2. a) The two parts of the cell cf. Fig.1. In the upper cover plate the diamond window is glued in. In the lower part the small O-ring, which bears the sample, located in the middle of the large sapphire window is shown. b) The cell in mounted state with the pressure inlet pointing to the left. c) The cell mounted to the *xy*-stage ready to use with the confocal microscope.

2.3. Objective

Due to the presence of a relatively thick diamond window with an extremely high index of refraction a long working distance objective with a correction collar was used. Our choice was Olympus SLC plan FL 40×/0.55, numerical aperture NA = 0.55, working distance WD = 7.7 mm and correction range = 0 - 2.6 mm (objective #1) and its successor, Olympus LUCPLFLN 40×/0.6 of NA = 0.6, WD = 3.0-4.2 mm and correction range = 0 - 2.0 mm (objective #2).

2.4. Confocal imaging

The sample was prepared by putting a drop of highly diluted water suspension of PS-FluoGreen particles of 0.606 μm diameter (Particles GmbH) on a cover glass (diamond) and waiting for a complete dry out. Confocal scans of the layer of particles settled on the surface were performed using an Olympus FV1000 system based on the inverted microscope Olympus IX81. The 488 nm Argon laser line was used for excitation. Objective #2 was applied in this experiment.

2.5. Particle tracking

Using video microscopic imaging techniques, submicron spheres can be localized in the focal plane typically with an accuracy to within tens of nanometres. Thus, particle tracking can give information on the mean square displacement of particles, provided the particles exact positions and trajectories can be obtained from the video sequences. For that purpose the algorithm developed by Crocker and Grier [24] was used. Then the measured displacement $\boldsymbol{r}(t)$-$\boldsymbol{r}(0)$ was related to the self diffusion coefficient D via the Einstein–Smoluchowski equation

$$\left\langle \left| \mathbf{r}(t) - \mathbf{r}(0) \right|^2 \right\rangle = 2dDt \tag{2}$$

where d is the dimension of the system (in our case d = 2) and D is the self-diffusion coefficient.

Transmission videomicroscopy was performed on an Axiovert Zeiss microscope equipped with objective #1 and operated by a Metamorph software. Series of images (movies) were taken with a Photonics Coolsnap HQ CCD camera with a pixel size of 0.27 μm. The time spacing between two consecutive frames ranged from 50 to 100 ms, i. e. the frame rate was between 10 and 20 per second. Each movie consisted of 400 frames. In each measurement three movies were taken. The average number of tracked particles was around 80.

2.4. Fluorescence correlation spectroscopy (FCS)

All FCS correlation functions were measured using the Zeiss ConfoCor 2 (Carl Zeiss AG, Jena, Germany) instrument (based on Axiovert 100M microscope) equipped with objective #2.

The experimental fluorescence correlation functions $G_{DT}(\tau)$ were analyzed using a model of free diffusion of small fluorescent dye-molecule with triplet contribution given by:

$$G_{DT}(\tau) = 1 + \frac{1}{N}\left[A\left(1+\frac{\tau}{\tau_D}\right)^{-1}\left(1+\frac{\tau}{\tau_D \kappa^2}\right)^{-1/2}\right]\left[1 - T + T\exp\left(-\frac{\tau}{\tau_T}\right)\right] \quad (3)$$

Here the indices refer to "D": diffusion, and "T": triplet term, while A and T are the respective amplitudes and τ_D, and τ_T are the respective characteristic times, N is the number of fluorescing particles in the confocal volume and $\kappa = \sigma_z / \sigma_{xy}$ is the structure parameter defined as the aspect ratio of the confocal volume described by semi axes σ_{xy}, σ_z [25] and the translational diffusion coefficient $D = \sigma_{xy}^2 / \tau_D$.

In our previous publications [5, 26] we have shown that the spherical aberration due to the diamond window thickness of 1 mm (refractive index n = 2.415) can be compensated by the correction collar of the LWD objective #1. We also demonstrated that this combination of objective #1 and a diamond window can be used for a successful FCS measurement. The efficiency of the LWD and immersion objectives in the FCS experiment was compared in detail earlier [5].

In Fig. 3 we show the normalized FCS correlation functions measured for Alexa488 solution in water using the objective #2. As one can see in Fig. 3, the shape of both correlation functions is identical resulting in the same value of the correlation time. The number of fluorescent molecules in the confocal volume, N, obtained from the amplitude of the correlation functions is slightly different indicating a small increase of the size of the confocal volume in the z-direction, resulting in a small increase of the structure parameter κ. Similar effects were discussed before [27, 28]. Molecular brightness (CPM) measured with a 1 mm diamond window is lower than that measured with a standard coverglass but still sufficient to perform accurate FCS measurements.

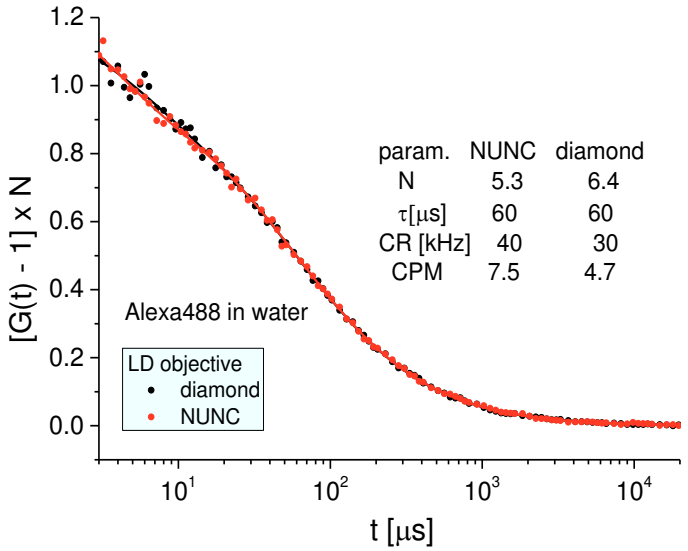

Figure 3. Normalized FCS correlation functions of Alexa488 water solution measured in cells with objective #2 and diamond window (black points) and cover glass (NUNC) window (red points). The values of the count rate (CR) and the values of N, τ and CPM obtained from fits using Eq. 3 for diamond and coverglass window, respectively, are indicated in the figure.

A similar comparison of the correlation functions measured for Rhodamine 6G water solution using objective #1 with coverglass and 1 mm diamond windows is shown in the Supplementary material in Fig. S1.

Thus, we can conclude that both objectives #1 and #2 can be used for successful FCS experiments with high pressure cells having a 1 mm thick diamond widow.

3. Results and discussion

3.1. Confocal imaging using the high pressure cell

Confocal images of PS spheres with 0.6 μm diameter lying on a cover glass of ~0.15 mm thickness (left) and on a 1 mm diamond window (right) are shown in Fig. 4.

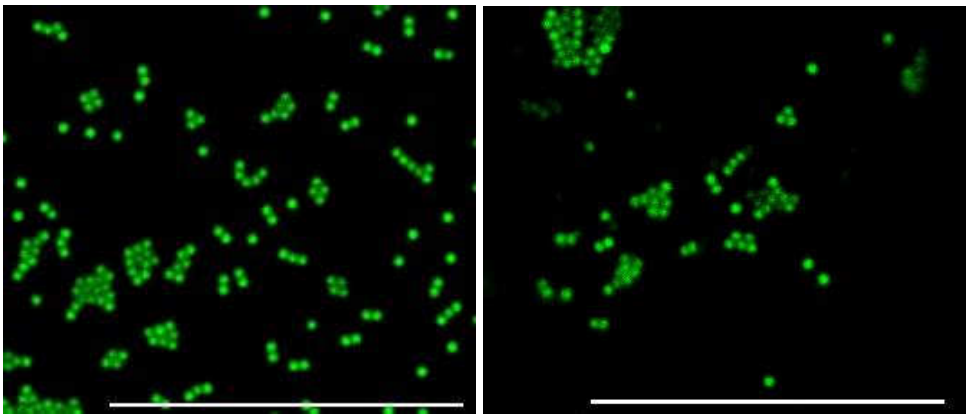

Figure 4. Fluorescence confocal scan images of 600 nm diameter labeled PS beads (MicroParticles GmbH): a) on a cover glass, b) on a diamond window. The scale bars represent 20 μm.

The size of the spheres was chosen such that they can hardly be imaged with the resolution offered by objective #2 and any optical mismatch should result in a strong deterioration of the particle image as well as the image brightness. Both in the case of the sample placed on a cover glass and on the diamond window the crucial condition to obtain an undistorted and bright image was the correct setting of the correction collar of the objective. Wrong position of that collar resulted in an order of magnitude weaker signal and significantly blurred image. The two pictures shown in Fig. 4 were obtained in identical experimental conditions concerning the excitation power and detector sensitivity. It is clear that practically identical images were obtained, despite the very high refractive index of the diamond and despite the large thickness of that window.

3.2. Particle tracking: Effect of high pressure on tracer diffusion of silica nanoparticles in ethanol and ethanol/water mixture – the nanoviscosity $\eta(P, T)$

In order to demonstrate the applicability of our set-up for high pressure experiments a 0.02 wt% dilute solution of stearyl coated silica spheres of 0.395 μm diameter in water/ethanol mixtures was measured in the transmission mode. For this low concentration the measured diffusion coefficient was practically equal to the value D_0 extrapolated to zero

nanoparticle concentration. From previous measurements of the radius of silica spheres in toluene as a function of pressure by means of small angle neutrons scattering (SANS), we have shown that the silica sphere size is practically pressure independent [29]. Thus, from the D_0 value the nano-viscosity can be obtained by applying the Stokes–Einstein relation:

$$D_0(P,T) = \frac{kT}{6\pi\eta(P,T)r} \tag{4}$$

Here r is the hydrodynamic radius of the diffusing particle, $\eta(P,T)$ is the pressure and temperature dependent viscosity, and k is the Boltzmann constant. For a water/ethanol mixture it is known that D exhibits a large pressure effect depending on the water to ethanol ratio. This reflects, contrary to regular liquids like toluene for example, the anomaly of the water viscosity and is explained in terms of the special water structure possessing hydrogen bonds. Specifically, within our observed pressure range [30] the viscosity of water and hence the diffusion coefficient of suspended colloids at ambient temperature do not depend on pressure. In fact the viscosity may even exhibit a minimum depending on pressure and temperature and reflects thus the water structure anomaly [30]. Adding more and more ethanol to water breaks the water structures based on hydrogen bonding and leads in the end to the viscosity/pressure behaviour of regular liquids, being intuitively characterized by an increase of the viscosity with increasing pressure. For pure ethanol the increase of η between 1 and 100 MPa is about 40%. For a 50/50 (v/v) mixture of water and ethanol it is still 20%.

We have chosen the 100% ethanol and 50/50 mixture of water and ethanol as examples to show the feasibility of our data evaluation and hence applicability of our high pressure microscopy device.

Typical MSD data obtained for the 100% ethanol sample for three pressure values is shown in Fig. 5. From initial slopes of the mean square displacement (MSD) versus time we obtained the translational diffusion coefficient D values using Eq. 2.

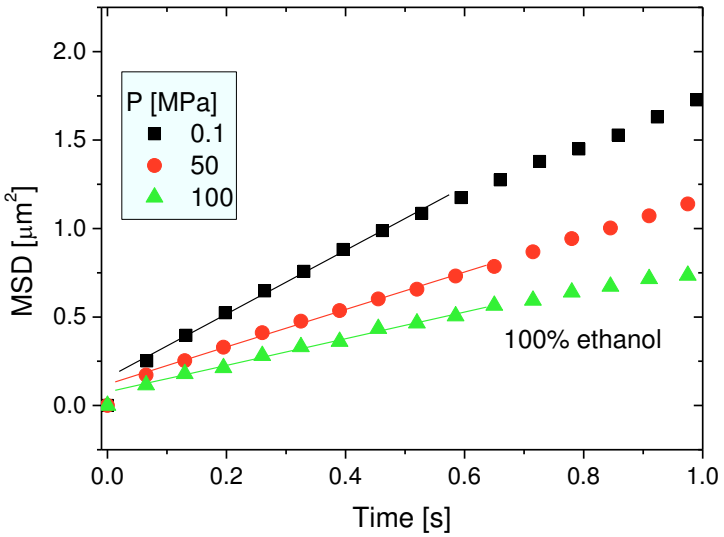

Figure 5. Mean square displacement MSD of test silica spheres in 100% ethanol as a function of pressure. From the initial slopes as shown in the Figure, D is calculated according to Eq. 2.

From the obtained $D^T(P)$ dependence the viscosity $\eta_{PT}(P)$ was calculated using the SE relation (Eq. 4). Identical procedure was performed for the same particles suspended in 50/50 ethanol/water mixture. The viscosities of the two samples are plotted versus pressure in Fig. 6 together with the rheological viscosity $\eta_{rheo}(P)$ data from literature [31, 32].

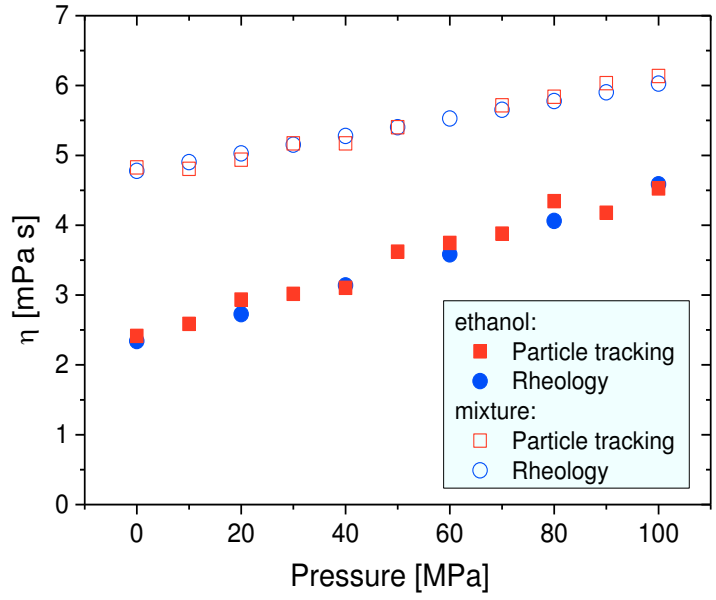

Figure 6. Comparison of $\eta_{PT}(P)$ calculated from particle tracking experiments at 20ºC in ethanol and in 50/50 ethanol/water mixture with literature rheological data of $\eta_{rheo}(P)$ for ethanol [31] and for the mixture [32].

We see that our method correctly reproduces the trend and is capable to determine $\eta_{PT}(P)$ within an accuracy of ±5%. Our method works sufficiently well and can give access to MSD, and hence to $D^T(P)$ and $\eta_{PT}(P)$ data under pressure which is otherwise difficult to obtain.

3.3. FCS: effect of high pressure and temperature on the tracer diffusion of a dye in OTP/BMPC mixture

Typical FCS correlation functions measured for the OTP/BMPC mixture at a temperature of 45ºC and at high pressures from 12 MPa to 73.5 MPa are shown (points) in Fig. 7. The solid red lines represent fits of Eq. 3 to the data. As one can see the shape of the experimental correlation functions is well described by Eq. 3.

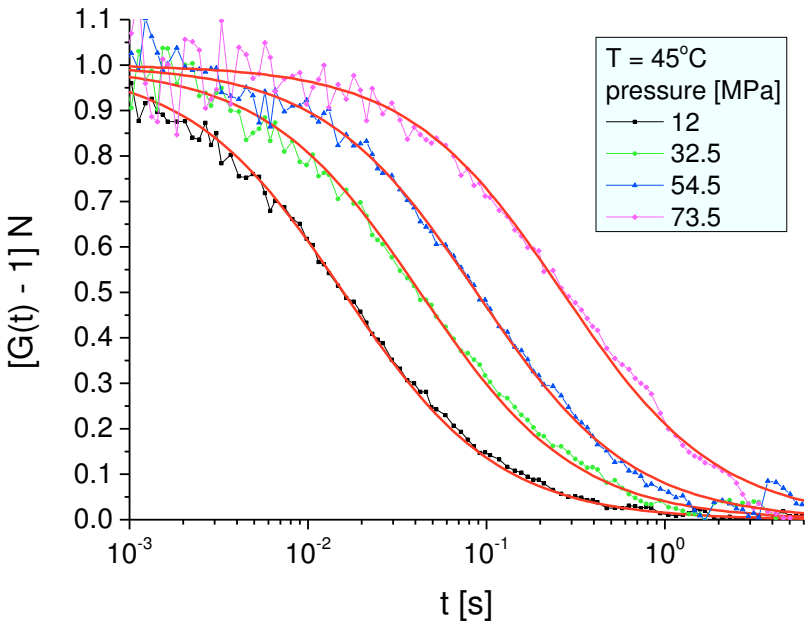

Figure 7. The normalized experimental FCS correlation functions measured for OTP/BMPC mixture at a temperature of 45ºC. The pressures are indicated in the figure. The solid red lines correspond to the fits of Eq. 3 to the data.

The FCS correlation times τ_{diff} obtained for the OTP/BMPC mixture are plotted vs. pressure for four temperatures from 25.5 to 55 ºC in Fig. 8.

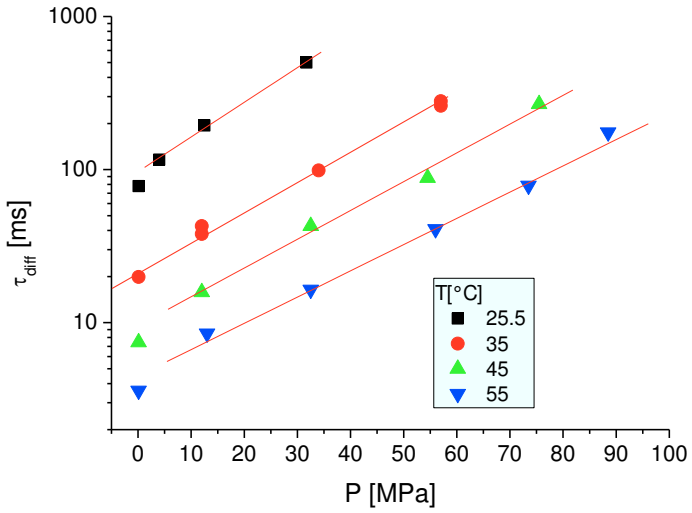

Figure 8. The correlation times τ_{diff}, obtained from the fit of Eq.3 to the FCS correlation functions measured at temperatures of 25.5, 35, 45 and 55ºC (different symbols explained in the figure), plotted vs. pressure. The solid lines are to guide the eye.

These correlation times correspond to the tracer translational diffusion of the dye over the distance of the diameter of the confocal volume σ_{xy}.

3.4. Density scaling of the *P*,*T*-dependent data for van der Waals glass forming liquids (OTP and OTP/BMPC mixture)

It was shown [33, 34] that the density scaling applies to the reduced quantities of the viscosity η, structural relaxation time τ and diffusion coefficient D, defined as :

$$\begin{aligned} \eta^* &= v^{2/3}(mkT)^{-1/2}\eta \\ \tau^* &= v^{-1/3}(kT/m)^{1/2}\tau \\ D^* &= v^{-1/3}(kT/m)^{-1/2}D \end{aligned} \qquad (5)$$

where v and m are the molecular volume and mass, respectively, and k is the Boltzmann constant.

The density scaling exponent γ is related to the steepness of the intermolecular repulsive inverse power law potential [35 – 39]. It is expected that the scaling exponent is the same for different experimental methods and probes and both the scaling function and the scaling exponent depend only on the material. In order to make the comparison more straightforward we have converted the translational self diffusion coefficient of the fluorescent dye, measured

by means of FCS, to nano-viscosity using the Stokes-Einstein equation (Eq. 4). Fig. 9 shows the reduced (according to Eq. 5) FCS correlation times τ^*_{FCS} which are related to the translational self diffusion coefficient D^T of the fluorescent probe: $\tau_{FCS} = <\sigma_{xy}^2>/D^T$ (σ_{xy} is the confocal volume radius) and taken from literature DLS correlation times τ_{DLS} [40]. The τ_{DLS} is the rotational relaxation time related to the rotational diffusion coefficient D^R by: $\tau_{DLS} = 1/(6D^R)$. The solid line in this figure represents the rheological viscosity taken from literature [41 – 43, 5] which consists of several sections as discussed in detail in our previous publication [5].

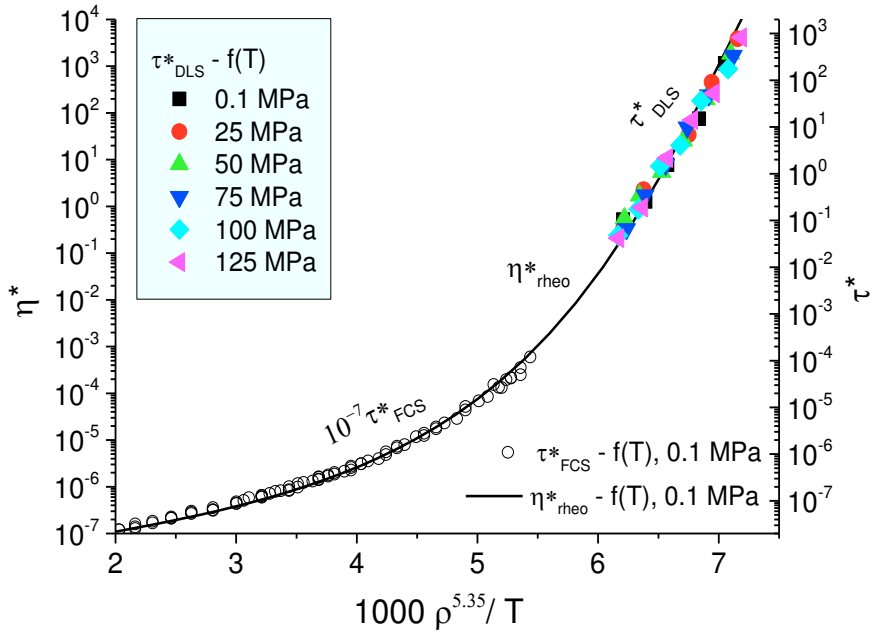

Figure 9. Density scaling of the reduced (Eq. 5) quantities for OTP: τ^*_{FCS} obtained from our FCS measurements [5] compared with the literature data of τ^*_{DLS} [40] and η_{rheo} [literature in Ref. 5]. The OTP density was calculated according to the equation of state taken from [6].

The scaling exponent obtained for all the OTP data in Fig. 9 using the new equation of state (EoS) [6] amounts to $\gamma = 5.35$. Thus, for OTP the density scaling works not only for rotational relaxation and viscosity, as it was shown in [6] but also for translational diffusion at temperatures $T > 1.2\ T_g$. In our previous publication [5] we have shown that the nano-viscosity calculated from the translational tracer diffusion coefficient of the fluorescent probe

using the SE relation measured by means of FCS not only scales with the macroscopic viscosity, but these two viscosities are equal. That means that in the temperature range $T > 1.2\ T_g$ the SE relation is valid.

It was shown before [44] that the scaling exponent might be different for unreduced and reduced quantities and, additionally, might depend on the experimental method. In Fig. S2 in Supplementary Material we show that in the case of OTP the density scaling of reduced and unreduced values results in the same scaling exponent.

The density scaling for OTP was first performed [7] using the PVT data of Naoki and Koeda [45] and the scaling exponent $\gamma = 4$ was obtained. In Fig. S3 in the Supplementary Material we present the density scaling of the same reduced and unreduced OTP data as in Fig. S2 but, this time, using the old PVT data [45]. As one can see both scaling plots are equally good.

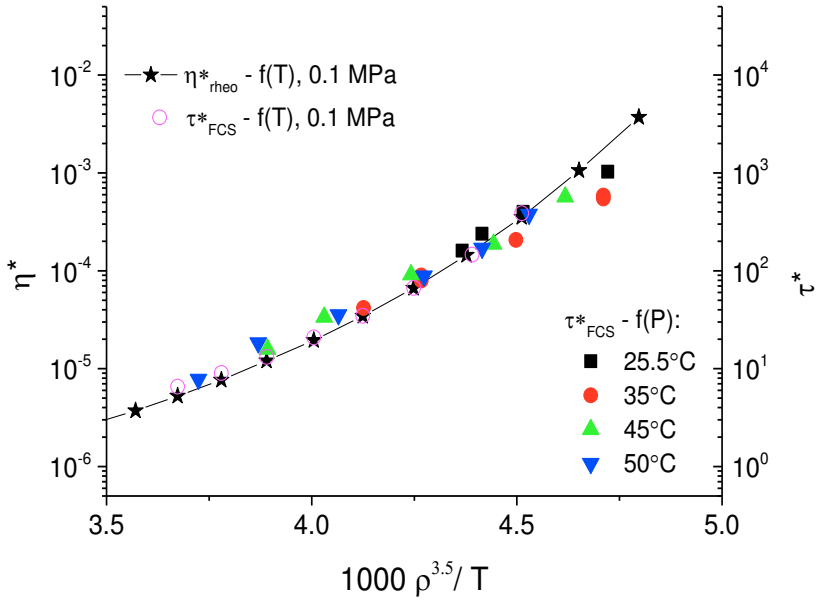

Figure 10. The reduced (Eq. 5) quantities: $\tau^*_{FCS}(P,T)$ obtained from the FCS measurements and the rheological viscosity $\eta^*_{rheo}(T)$ plotted vs. the scaling parameter $\rho^{3.5}/T$ for the OTP/BMPC mixture. The OTP and BMPC densities were calculated according to the equations of state taken from [6] and [46], respectively.

A similar density scaling of the FCS and viscosity data was also performed for the OTP/BMPC mixture. In Fig. 10 the reduced (Eq.5) values of the temperature and pressure dependent relaxation times $\tau^*_{FCS}(P,T)$ from Fig. 8 related to the translational tracer diffusion

coefficient, and the rheological viscosity $\eta_{rheo}(T)$ measured at 0.1 MPa at different temperatures are plotted versus the scaling parameter $\rho^{3.5}/T$.

Also for the OTP/BMPC mixture the temperature and pressure dependent relaxation time $\tau^*_{FCS}(P,T)$ obtained from the FCS measurements scale in the same way as the rheological viscosity $\eta^*_{rheo}(T)$ with the scaling exponent equal to 3.5. Additionally, as it was shown partly earlier [5], the nano-viscosity η_{FCS} calculated from the FCS data using the SE relation is equal to the rheological viscosity η_{rheo} without any need of scaling. It is illustrated by plotting the reduced viscosities η^* as a function of the scaling parameter in Fig. S4 in the Supplementary Material. That indicates the validity of the SE relation for this material in the temperature and pressure ranges studied.

4. Conclusions

We have shown that a combination of a novel cell for high pressure microscopy using a flat diamond window and a long working distance objective equipped with a correction collar for thick cover glasses can be used for high resolution microscopy and fluorescence correlation spectroscopy for pressures up to 100 MPa. Using this setup we show that the pressure dependent nano-viscosity of ethanol and ethanol/water mixture obtained from the tracer diffusion coefficient of silica spheres measured by PT and calculated using the SE relation is identical to the macroscopic viscosity.

Our T and P dependent FCS measurements resulted in the nano-viscosity of the OTP/BMPC mixture which was equal to the macro-viscosity obtained from rheology at $T > 1.2\ T_g$.

We also show that the nano-viscosity of OTP and OTP/BMPC mixture obtained from the translational diffusion times measured by means of FCS at different P and T obeys the same density scaling as the macro-viscosity and rotational relaxation times at $T > 1.2\ T_g$. Thus, at temperatures $T > 1.2\ T_g$ the translational diffusion measured by means of FCS, in agreement

with results of other methods, does not decouple from the macroscopic viscosity despite the existence of structural and dynamic heterogeneities in supercooled liquids.

The possibility of performing pressure and temperature dependent investigations of dynamics of a liquid by means of PT and FCS opens new perspectives for experimental studies of heterogeneous dynamics in supercooled liquids.

Supplementary Material

The Supplementary Material contains four figures. Fig. S1 shows FCS correlation functions obtained using Objective #1 for a dilute Rhodamine 6G solution on a cover glass and on a diamond plate. In Figs. S2 and S3 we present the density scaling of the same reduced and unreduced OTP data using PVT data from references 10 and 38, respectively. Fig. S4 shows the scaling plot of the nano-viscosity $\eta^*_{FCS}(P,T)$ of the OTP/BMPC mixture calculated from the FCS data.

Acknowledgement

We gratefully acknowledge financial support by the grant no. 2013/09/B/ST3/01678 of the Polish National Science Centre and the support for M. R. from the European Network of Excellence SoftComp.

References

[1] L. Brethier, G. Biroli, *Rev. Mod. Phys.* **83** 587-645 (2011).

[2] M. D. Ediger, *Annu. Rev. Phys. Chem.* **51**, 99-128 (2000).

[3] L. J. Kaufman, *Annu. Rev. Phys. Chem.* **64**, 177-200 (2013).

[4] K. Paeng, H. Park, D. T. Hoang, and L. J. Kaufman, *PNAS* **112** 4952-4957 (2015).

[5] A. Połatynska, K. Tomczyk, M. Pochylski, G. Meier, J. Gapinski, E. Banachowicz, T. Sliwa, and A. Patkowski, *J. Chem. Phys.* **146**, 084506 (2017)

[6] R. Casalini, S. S. Bair, and C. M. Roland, *J. Chem. Phys.* **145**, 064502 (2016)

[7] C. Dreyfus, A. Le Grand, J. Gapinski, W. Steffen, and A. Patkowski, *Eur. Phys. J. B* **42**, 309 (2004)

[8] M. Hartmann, F. Pfeifer, G. Dornheim and K. Sommer *Chemie Ingenieur Technik* **75**, 1763 (2003)

[9] J. D. Müller and E. Gratton, *Biophys. J.* **85**, 2711 (2003)

[10] B. Frey, M. Hartmann, M. Herrmann, R. Meyer-Pittroff, K. Sommer and G. Bluemelhuber, *Microsc. Res. Tech*. **69**, 65 (2006)

[11] H. Vass, S. L. Black, E. M. Herzig, F. B. Ward, P. S. Clegg and R. J. Allen, *Rev. Sci. Instrum.* **81**, 053710 (2010)

[12] H. Vass, S. L. Black, C. Flors, D. Lloyd, F. B. Ward, and R. J. Allen, *Appl. Phys. Lett*, **102**, 154103 (2013)

[13] P. Holmqvist, M. Ratajczyk, G. Meier, H. H. Wensink and M. P. Lettinga, *Phys. Rev. E* **80**, 031402 (2009)

[14] J. Kohlbrecher, A. Bollhalder, R. Vavrin and G. Meier, *Rev. Sci. Instrum.* **78**, 125101 (2007)

[15] G. Meier and H. Kriegs, *Rev. Sci. Instrum*. **79**, 013102 (2008)

[16] J. Szymański, A. Patkowski, A. Wilk, P. Garstecki and R. Hołyst, *J. Phys. Chem. B* **110**, 25593-25597 (2006)

[17] T. K alwarczyk, N. Ziebacz, A. Bielejewska, E. Zaboklicka, K. Koynov, J. Szymanski, A. Wilk, A. Patkowski, J. Gapiński, H.-J. Butt, R. Holyst, *Nano Lett.* **11**, 2157 (2011)

[18] G. Meier, B. Gerharz, D. Boese, E. W. Fischer, *J. Chem. Phys.* **94**, 3050 (1991)

[19] E. P.Petrov, P. Schwille, State of the art and novel trends in fluorescence correlation spectroscopy. in Standardization and Quality Assurance in Fluorescence Measurements: State of the Art and Future Challenges. U. Resch-Genger, editor. Springer, Berlin, Heidelberg, New York 2008

[20] W. Strober, A. Fink, and E. Bohn. *J. Colloid Interface Sci.*, **26**, 62 (1968)

[21] A. K. van Helden, J. W. Jansen, and A. Vrij, *J. Coll. Interface Sci.* **81**, 354 (1981)

[22] J. Kohlbrecher, J. Buitenhuis, G. Meier, and M. P. Lettinga, *J. Chem. Phys.* **125**, 0447151 (2006)

[23] N. S. Isaacs, Liquid Phase High Pressure Chemistry, Chapter 1, John Wiley & Sons Inc 1981

[24] J. C. Crocker and D. G. Grier, *J. Coll. Int. Sci*. **179**, 298 (1996)

[25] R. Rigler and E. S. Elson (eds.) *Fluorescence Correlation Spectroscopy*, chapter 22, Springer, Berlin 2001

[26] E. Banachowicz, A. Patkowski, G. Meier, K. Klamecka, and J. Gapiński, *Langmuir* **30**, 8945 (2014)

[27] A. Egner and S. W. Hell, *Handbook of biological confocal microscopy*, J. B. Pawley (ed.), chapter 20, Springer, Singapore 2006

[28] R. Biehl and T. Palberg, *Rev. Sci. Instum.* **75**, 906 (2004)

[29] G. Meier, R. Vavrin, J. Kohlbrecher, J. Buitenhuis, M. P. Lettinga and M. Ratajczyk, *Meas. Sci. Technol.* **19**, 034017 (2008)

[30] K. E. Bett and J. B. Cappi *Nature* **207**, 620 (1965)

[31] C. K. Zěberg-Mikkelsen, A. Baylaucq, G. Watson and C. Boned, *Int. J. Thermophys*. **26**, 1289 (2005)

[32] Y. Tanaka, T. Yamamoto, Y. Satomi, H. Kubota and T. Makita, *Rev. Phys. Chem. Jap*. **47**, 12 (1977)

[33] Y. Hiwatari, H. Matsuda, T. Ogawa, N. Ogita, and A. Ueda, *Prog. Theor. Phys.* **52**, 1105 (1974)

[34] W. G. Hoover and M. Ross, *Contemp. Phys.* **12**, 339 (1971)

[35] L. Bohling, N. P. Bailey, T. B. Schroder, and J. C. Dyre, *J. Chem. Phys.* **140**, 124510 (2014)

[36] U. R. Pedersen,T. B. Schroder, and J. C. Dyre, *Phys. Rev. Lett.* **105**, 157801 (2010)

[37] N. P. Bailey, U. R. Pedersen, N. Gnan, T. B. Schroder, and J. C. Dyre, *J. Chem. Phys.* **129**, 184507 (2008)

[38] D. Coslovich and C. M. Roland, *J. Phys. Chem. B* **112**, 1329 (2008)

[39] C. M. Roland, S. Bair, and R. Casalini, *J. Chem. Phys.* **125**, 124508 (2006)

[40] G. Fytas, Th. Dorfmuller, and C. H. Wang, *J. Phys. Chem.* **87**,5041 (1983)

[41] M. Cukierman, J. W. Lane, and D. R. Uhlmann, *J. Chem. Phys.* **59**, 3639 (1973)

[42] E. Mc Laughlin and A. R. Ubbelohde, *Trans. Faraday Soc.* **54**, 1804 (1958)

[43] R. J. Greet and J. H. Magill, *J. Phys. Chem.* **71**, 1746 (1967)

[44] D. D. Fragiadakis and C.M. Roland, *J. Chem. Phys.* **134**, 044504 (2011)

[45] M. Naoki and S. Koeda, *J. Phys. Chem.* **93**, 948 (1989)

[46] M. Paluch, C.M. Roland, R. Casalini, G. Meier and A. Patkowski, *J. Chem. Phys.* **118**, 4578-4582 (2003)

Figure Captions

Figure 1. Schematic sketch of the cell. 1: cell body, 2: cover plate, 3: diamond window, 4: O-ring to embed the sample, 5: groove for the large O-ring, 6: sapphire/glass window, 7: holes for screws, 8: gap for pressurizing medium.

Figure 2. a) The two parts of the cell cf. Fig.1. In the upper cover plate the diamond window is glued in. In the lower part the small O-ring, which bears the sample, located in the middle of the large sapphire window is shown. b) The cell in mounted state with the pressure inlet pointing to the left. c) The cell mounted to the *xy*-stage ready to use with the confocal microscope.

Figure 3. Normalized FCS correlation functions of Alexa488 water solution measured in cells with objective #2 and diamond window (black points) and cover glass (NUNC) window (red points). The values of the count rate (CR) and the values of N, τ and CPM obtained from fits using Eq. 3 for diamond and coverglass window, respectively, are indicated in the figure.

Figure 4. Fluorescence confocal scan images of 600 nm diameter labeled PS beads (MicroParticles GmbH): a) on a cover glass, b) on a diamond window. The scale bars represent 20 μm.

Figure 5. Mean square displacement MSD of test silica spheres in 100% ethanol as a function of pressure. From the initial slopes as shown in the Figure, *D* is calculated according to Eq. 2.

Figure 6. Comparison of $\eta_{PT}(P)$ calculated from particle tracking experiments at 20ºC in ethanol and in 50/50 ethanol/water mixture with literature rheological data of $\eta_{rheo}(P)$ for ethanol [31] and for the mixture [32].

Figure 7. The normalized experimental FCS correlation functions measured for OTP/BMPC mixture at a temperature of 45ºC. The pressures are indicated in the figure. The solid red lines correspond to the fits of Eq. 3 to the data.

Figure 8. The correlation times τ_{diff}, obtained from the fit of Eq.3 to the FCS correlation functions measured at temperatures of 25.5, 35, 45 and 55ºC (different symbols explained in the figure), plotted vs. pressure. The solid lines are to guide the eye.

Figure 9. Density scaling of the reduced (Eq. 5) quantities for OTP: τ^*_{FCS} obtained from our FCS measurements [5] compared with the literature data of τ^*_{DLS} [40] and η_{rheo} [literature in Ref. 5]. The OTP density was calculated according to the equation of state taken from [6].

Figure 10. The reduced (Eq. 5) quantities: $\tau^*_{FCS}(P,T)$ obtained from the FCS measurements and the rheological viscosity $\eta^*_{rheo}(T)$ plotted vs. the scaling parameter $\rho^{3.5}/T$ for the OTP/BMPC mixture. The OTP and BMPC densities were calculated according to the equations of state taken from [6] and [46], respectively.